Applied Surface Science 255 (2009) 9420–9424

Contents lists available at ScienceDirect

Applied Surface Science

journal homepage: www.elsevier.com/locate/apsusc

Influence of oxygen growth pressure on laser ablated Cr-doped In_2O_3 thin films

N.B. Ukah, R.K. Gupta *, P.K. Kahol, K. Ghosh

Department of Physics, Astronomy, and Materials Science, Missouri State University, Springfield, MO 65897, USA

ARTICLE INFO

Article history:
Received 2 June 2009
Received in revised form 16 July 2009
Accepted 16 July 2009
Available online 23 July 2009

Keywords:
Indium oxide
Chromium
Transparent conductor
Mobility

ABSTRACT

We present a systematic investigation of the effects of oxygen growth pressure on the structural, optical, and electrical properties of In_2O_3:Cr thin films grown by pulsed laser deposition. X-ray diffraction analysis showed increases in lattice constant from 10.103 Å to 10.337 Å, and in particle size from 13.9 nm to 35.5 nm as the oxygen growth pressure increased from 7.5×10^{-6} Torr to 7.5×10^{-3} Torr, respectively. The observed shift in the X-ray diffraction peaks to lower angles was assumed to be caused by the reduction in the lattice defect density, precisely oxygen vacancies. The optical transparency increased with partial oxygen pressure (P_{O_2}), and an average transmittance of ~85% was obtained at 7.5×10^{-3} Torr. The films are highly conducting with resistivity as low as 2×10^{-4} Ω cm and mobility as high as 133 cm/V s. Temperature dependent resistivity measurements in the $45 < T < 300$ K temperature range reveal that films grown at $7.5 \times 10^{-6} \leq P_{O_2} \leq 7.5 \times 10^{-4}$ Torr exhibit negative temperature coefficient of resistivity (TCR) below approximately $T = 60$ K, $T = 120$ K, $T = 160$ K; then positive TCR in the temperature intervals $60 < T < 300$ K, $120 < T < 300$ K, and $160 < T < 300$ K, respectively. This suggests that two disparate mechanisms govern electrical dc transport in the two temperature regions. Film grown at P_{O_2} of 7.5×10^{-3} Torr displayed typical semiconducting behavior with negative TCR in the whole temperature region.

1. Introduction

Until recently, semiconductor research has been restricted to the conventional semiconductor electronics, which is based only on the manipulation of the charge of the electron leaving out the spin. Owing to the realization of the need to manipulate both the spin and the charge of the electron arising from its relevance to spin electronics, intense research efforts have been directed at realizing ferromagnetic semiconductor materials with Curie temperatures (T_C), especially above room temperature [1,2]. It turns out that dilute magnetic semiconductor (DMS) materials formed when transition metals are doped into a semiconductor host lattice such as Cr on AlN or GaN, are potential candidates for the development of electro-magneto-optic devices [2]. This research field (DMS) got a boost with the theoretical prediction of room temperature ferromagnetism in Mn-doped ZnO and SnO_2 coupled with the discovery of ferromagnetism in Mn-doped InAs and GaAs; although, at Curie temperatures less than room temperature [3,4]. The first reports of ferromagnetic ordering in oxides were for Co-doped TiO_2 (anatase), ZnO, and SnO_2 [5–7]. The need to develop next generation multifunctional devices necessitates the search for semiconducting oxides with tunable carrier density, high mobility and optical transparency.

Indium oxide (In_2O_3) is a transparent, n-type material with inherent oxygen deficiencies whose conductivity can be effectively tuned by tuning the oxygen vacancies or by Sn doping [8]. Compared with other transition metals, Cr has large magnetic moment in the ionic state and unlike Co, observation of ferromagnetism due to Cr clustering is ruled out since trace amounts of Cr clusters are superparamagnetic, while bulk Cr is antiferromagnetic. Only two demonstrations of high temperature ferromagnetism in Cr-doped In_2O_3 have been reported; though, without detailed structural and optical investigations. Philip et al. [9] have reported high temperature ferromagnetism in Cr-doped In_2O_3 thin films grown by co-evaporation technique, and proposed that carrier-mediation is responsible for the observed magnetic behavior. According to their report, the electrical and magnetic behavior of Cr-doped In_2O_3-ranging from ferromagnetic metal-like ($n_c = 3 \times 10^{20}$ cm^{-3}, $M_s = 1.5$ μ_B/Cr) to ferromagnetic semiconducting ($n_c = 1 \times 10^{20}$ cm^{-3}, $M_s = 1.25$ μ_B/Cr) to paramagnetic insulator ($n_c = 9 \times 10^{18}$ cm^{-3}) can be controllably tuned by varying the defect concentration (oxygen vacancies) in these films. Kharel et al. [10] have also reported the demonstration of room temperature ferromagnetism in spin-coated Cr-doped In_2O_3 thin films and bulk samples only after high vacuum annealing of the samples. The carrier densities and saturation magnetization values for the thin film and bulk samples are 6.6×10^{17} cm^{-3} (0.22 μ_B/Cr)

* Corresponding author. Tel.: +1 417 836 6298; fax: +1 417 836 6226.
E-mail addresses: ndubuisi13@missouristate.edu (N.B. Ukah), ramguptamsu@gmail.com (R.K. Gupta).

0169-4332/$ – see front matter © 2009 Elsevier B.V. All rights reserved.
doi:10.1016/j.apsusc.2009.07.045

and 7×10^{18} cm^{-3} (0.008 μ_B/Cr), respectively. Average optical transparency values of ~88% and ~80% have been reported for Ti-doped In_2O_3 and Zn-doped In_2O_3 thin films, respectively [11,12]. D.C. magnetron sputtering technique has been used to fabricate tungsten doped indium oxide thin films having carrier concentration of 2.9×10^{20} cm^{-3} and mobility of 73 cm^2/V s [13]. Other techniques such as thermal evaporation [14], rf magnetron sputtering [15], sol–gel [16], and pulsed laser deposition [17] have also been used for deposition of indium oxide films. This literature survey suggests that electrical, optical as well as magnetic properties of indium oxide thin films are dependent on the growth technique. Among these techniques, pulsed laser deposition has the advantage of maintaining target composition in the deposited film. It also enables the deposition of high quality films due to the high kinetic energy of atoms and ionized species in the laser-produced plasma [18]. In this paper, we aim to understand the structural, optical, and electrical transport property relationships of In_2O_3:Cr thin films grown under different partial oxygen pressures using pulsed laser deposition (PLD) technique, which would be critical in explaining any future observed magnetic behavior.

2. Experimental details

A chromium-doped indium oxide (In_2O_3:Cr) target with 2.5 at.% chromium was prepared by standard solid-state reaction method using high purity In_2O_3 (99.999%) and Cr_2O_3 (99.8%). Required amounts of In_2O_3 and Cr_2O_3 were taken by molecular weight and mixed thoroughly. The well-ground mixture was heated in air at 800 °C for 12 h. The powder mixture was cold-pressed using a hydraulic press at 15 ton load, and sintered in air at 800 °C for 12 h. Cr-doped In_2O_3 thin films were grown on *c*-plane sapphire substrates using pulsed laser deposition technique (KrF excimer laser, λ = 248 nm) for ~20 min at a substrate temperature of 400 °C. The laser was operated at a pulse rate of 10 Hz and energy of 300 mJ/pulse (spot size of 1 × 1 mm^2). The target to substrate distance was 5.0 cm. The deposition chamber was initially evacuated to a base pressure of $\sim 3.0 \times 10^{-6}$ Torr, followed with the introduction of oxygen gas in order to obtain the required growth pressures of 7.5×10^{-6} (Sample A) Torr, 7.5×10^{-5} (Sample B) Torr, 7.5×10^{-4} (Sample C) Torr, and 7.5×10^{-3} (Sample D) Torr. All samples were characterized with the Bruker AXS X-ray diffractometer using CuK_α radiation having a wavelength of 1.5406 Å. The surface morphology of the films was investigated using atomic force microscopy (Digital Instruments, Veeco-3100). The film thickness is approximately 100 nm. The optical transmittance measurements were made using ultra-violet visible spectrophotometer (Ocean Optics HR400). The resistivity and Hall effect measurements were carried out using the standard four-probe technique. All film resistivity was obtained from the average of measurements for each film. The magnetic field dependence of Hall effect was measured with the field applied perpendicular to the film surface in the Van der Pauw configuration. The Hall voltage was measured using a Keithley 182 voltmeter and current was supplied using the Keithley 230 current source. The conductivity for all samples was confirmed to be n-type from Hall effect measurements.

3. Results and discussion

In_2O_3 crystallizes in the cubic bixbyte structure with a lattice constant of 10.118 Å and a direct band gap of 3.75 eV [19]. The diffraction peaks (A–D) in Fig. 1 are for In_2O_3:Cr samples grown at 7.5×10^{-6} Torr, 7.5×10^{-5} Torr, 7.5×10^{-4} Torr, and 7.5×10^{-3} Torr of oxygen on sapphire substrates. The films are highly crystalline and in good agreement with the JCPDS file card no. 06-0416 for In_2O_3, all the films show peaks corresponding to In_2O_3 phase only, which suggests that Cr forms a solid solution with In_2O_3 in all our samples. It could be seen from Fig. 1 that not all the peaks are present. This is due to the preferential orientation of the films in the (2 2 2) plane. Such type of preferential growth has been also observed for tungsten doped In_2O_3 films grown on quartz substrate [20]. The peaks labeled 'S' correspond to the substrate. From the inset of Fig. 1, one notices an obvious shift of the diffraction peaks to lower angles with increasing partial oxygen pressure, which indicates an expansion in the lattice constant. There is an increase in lattice constant from 10.103 Å to 10.337 Å as the oxygen growth pressure increases from 7.5×10^{-6} to 7.5×10^{-3} Torr as shown in Fig. 2. For Sample A, it could be explained that the lattice distortion and consequent lower lattice constant value (10.103 Å) when compared with In_2O_3 (10.118 Å), is due to the incorporation of smaller Cr ions into the In sites of the In_2O_3 lattice [9]. A broadening of the (2 2 2) diffraction peaks due to the effects of strain and/or size, is also noticeable from the inset of Fig. 1. Sherrer's method was employed to estimate the particle sizes of the thin films using the relation [21]:

$$t = \frac{C\lambda}{\beta \cos \vartheta} \quad (1)$$

where β is the full width at half maximum (FWHM) of the XRD peak, λ is the X-ray wavelength, ϑ is the diffraction angle, and C is

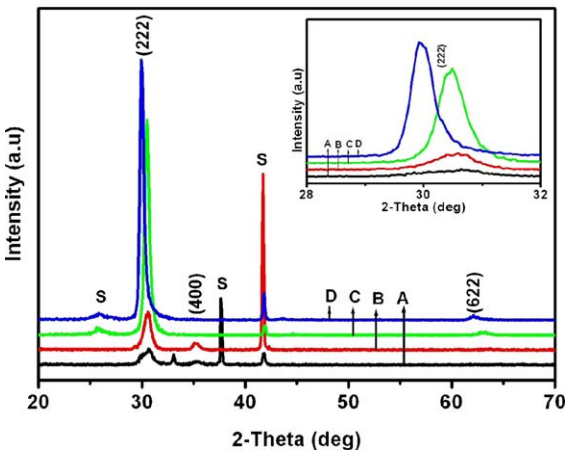

Fig. 1. X-ray diffraction pattern for films grown at partial pressures of (A) 7.5×10^{-6} Torr, (B) 7.5×10^{-5} Torr, (C) 7.5×10^{-4} Torr, and (D) 7.5×10^{-3} Torr of oxygen.

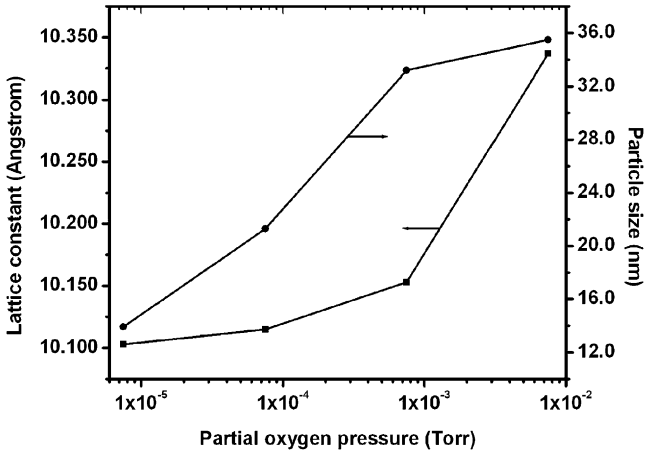

Fig. 2. Plots of lattice constant and particle size vs. partial oxygen pressure for In_2O_3:Cr films.

the correction factor which is taken as unity. The estimated particle sizes were determined using the (2 2 2) diffraction peaks and are shown in Fig. 2. The particle size varies from 13.9 nm to 35.5 nm with increase in partial oxygen pressure. Tsunekawa et al. [22] have reported an observed anomalous lattice expansion with decreasing particle size in oxide nanoparticles. Zhou and Hueber [19] have also correlated an observed lattice expansion and decrease in particle size in CeO_2 nanoparticles, with increased concentration of oxygen vacancies. In this work, our observed lattice expansion and increase in particle size with increased partial oxygen pressure is proposed to be due to the reduction in oxygen vacancies in these thin films. The shrinking of the full width at half maximum (FWHM) of the diffraction peaks with increase in partial oxygen pressure (inset of Fig. 1), an indication of improved crystallinity, independently supports the estimated particle sizes for the films. The FWHM of (2 2 2) decreases from 0.0108 rad to 0.0031 rad as the partial oxygen pressure increases from 7.5×10^{-6} Torr to 7.5×10^{-3} Torr.

Atomic force microscopy (AFM) was used to study the surface morphology of these films. Fig. 3 shows AFM images of In_2O_3:Cr samples grown at 7.5×10^{-5} Torr and 7.5×10^{-3} Torr of oxygen pressure. The scan was carried out in tapping mode. The spring constant of the cantilever was ~42 N/m. The cantilevered tip was oscillated close to the mechanical resonance frequency of the cantilever (typically, 200–300 kHz) with amplitudes ranging from

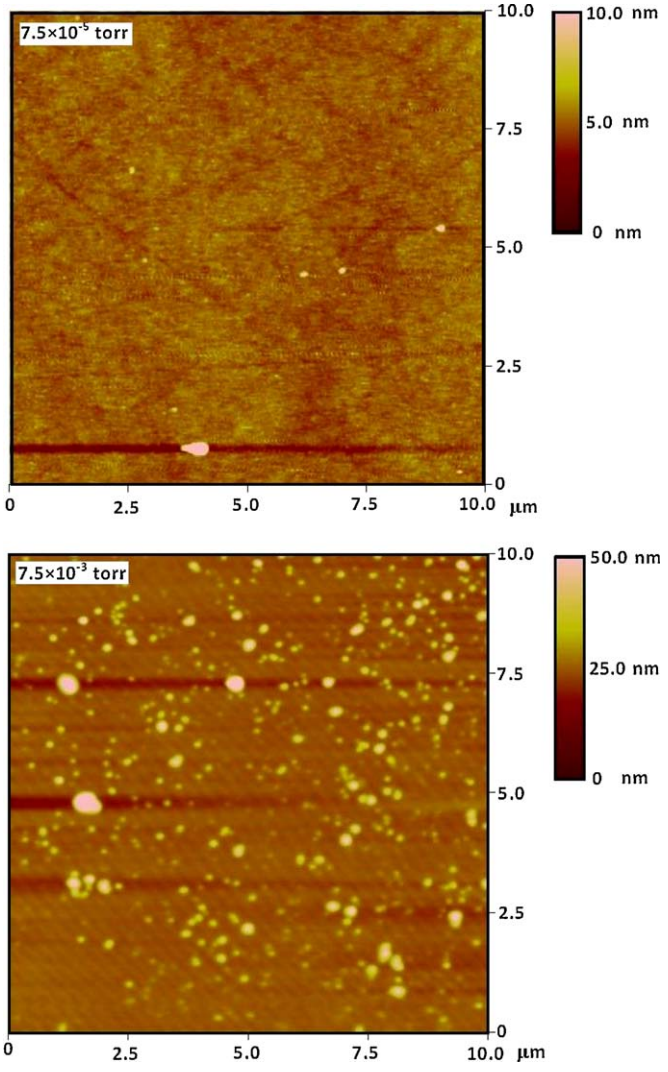

Fig. 3. AFM images of In_2O_3:Cr films grown at different oxygen partial pressure.

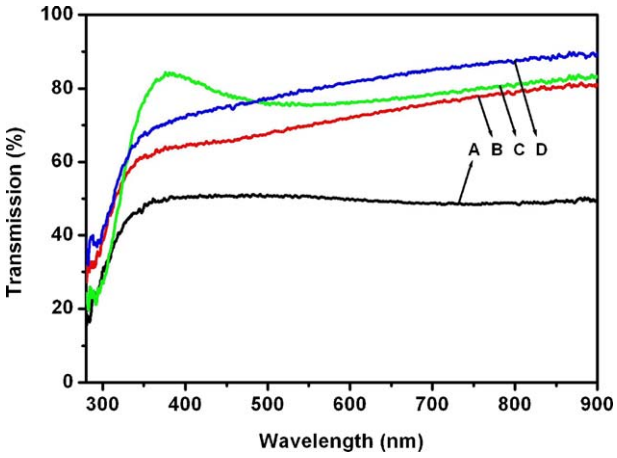

Fig. 4. Optical transmission spectra of In_2O_3:Cr films.

10 nm to 30 nm. It is observed that high oxygen pressure during growth of films produces rougher films with bigger particle size.

The optical transmission spectra of In_2O_3:Cr films are shown in Fig. 4. Optical transmittance is observed to be strongly dependent on the oxygen growth pressure. The average optical transparency is observed to increase from ~55% to ~85% as the partial oxygen pressure increased from 7.5×10^{-6} Torr to 7.5×10^{-3} Torr, respectively. According to the Drude model [23], the plasma frequency ω_p, responsible for the absorption peaks is given by:

$$\omega_p^2 = \frac{ne^2}{m^* \varepsilon_0} \tag{2}$$

where e is the electron charge, n is the electron density, ε_0 is the permittivity in free space, and m^* is the electron effective mass. In order to explain the observed optical behavior of our films, we employed the ionized impurity scattering model due to high carrier concentration of these films. Here, the frequency dependent relaxation time, which is usually introduced at $\omega > \omega_p/\sqrt{\varepsilon_\infty}$ is given by [24]:

$$\tau^{IIS}(\omega) = \tau_0 \left(\frac{\omega_p}{\sqrt{\varepsilon_\infty}}\right)^{-3/2} \omega^{3/2} \tag{3}$$

where $\omega_p/\sqrt{\varepsilon_\infty}$ is the screened plasma frequency. The decrease in the screened plasma frequency with increase in partial oxygen pressure, and consequent reduction in carrier concentration, results in increased relaxation time and reduced absorption. Hence, transparency is enhanced in the films. The optical transmittace (T), when reflectivity near the absorption edge is neglected is given by [12],

$$T = T_0 \exp(-\alpha d) \tag{4}$$

where α and d are the optical absorption coefficient and the film thickness, respectively. Estimates of the energy band gap, E_g of the films were obtained using the relation:

$$(\alpha h\upsilon)^2 = (h\upsilon - E_g) \tag{5}$$

where $h\upsilon$ is the photon energy. By an extrapolation of the linear region of $(\alpha h\upsilon)^2$ vs. $h\upsilon$ plot to the photon energy axis, the energy band gap, E_g can be obtained as shown in Fig. 5. A decrease of the energy band gap with partial oxygen pressure is observed. The observed decrease in the energy band gap from approximately 3.93 eV to 3.76 eV is traceable to improved crystal quality of the films with increase in oxygen growth pressure as seen from the XRD analysis, which gives rise to the reduction of the inter-atomic spacing as well as to the shifts of the absorption edges to longer wavelengths.

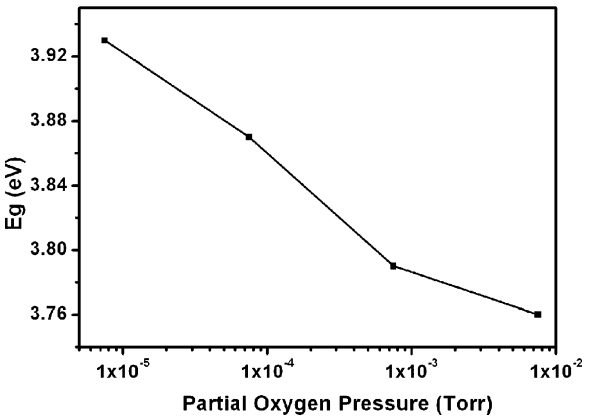

Fig. 5. Effect of partial oxygen pressure on band gap of In_2O_3:Cr films.

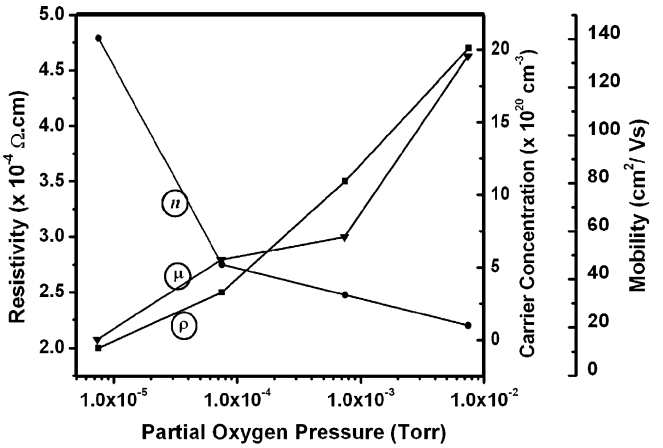

Fig. 6. Effect of partial oxygen pressure on electrical (a) resistivity, (b) carrier concentration, and (c) mobility of In_2O_3:Cr films.

The effect of oxygen partial pressure on electrical properties of these films is studied in details. From Fig. 6, it could be noticed that the resistivity and mobility of the films increase with increase in oxygen growth pressure. The resistivity of the films increases from $2 \times 10^{-4}\ \Omega$ cm to $4.7 \times 10^{-4}\ \Omega$ cm with increase in oxygen pressure from 7.5×10^{-6} Torr to 7.5×10^{-3} Torr, respectively. An improvement in mobility from 15 cm^2/V s to 133 cm^2/V s with increase in partial oxygen pressure from 7.5×10^{-6} Torr to 7.5×10^{-3} Torr is also observed. This observed increase in mobility is due to improvement in crystallinity and reduction in grain boundary scattering resulting from increase in grain size as corroborated by XRD analysis. On the other hand, the decrease in carrier concentration and consequent increase in resistivity of the films, with increasing partial oxygen pressure are brought about by the reduction in the defect density, specifically oxygen vacancies [9].

Temperature dependent resistivity measurements in the $45 < T < 300$ K temperature interval for the films reveal interesting behaviors as could be seen from Fig. 7. For films grown at lower oxygen pressure (Samples A–C), resistivity reaches a minimum at approximately $T = 60$ K, $T = 120$ K, and $T = 160$ K, respectively, and consequently exhibit negative temperature coefficient of resistivity (TCR) below these temperatures. The samples also exhibit metallic behavior and have positive TCR in the temperature ranges $60 < T < 300$ K, $120 < T < 300$ K, and $160 < T < 300$ K, respec-

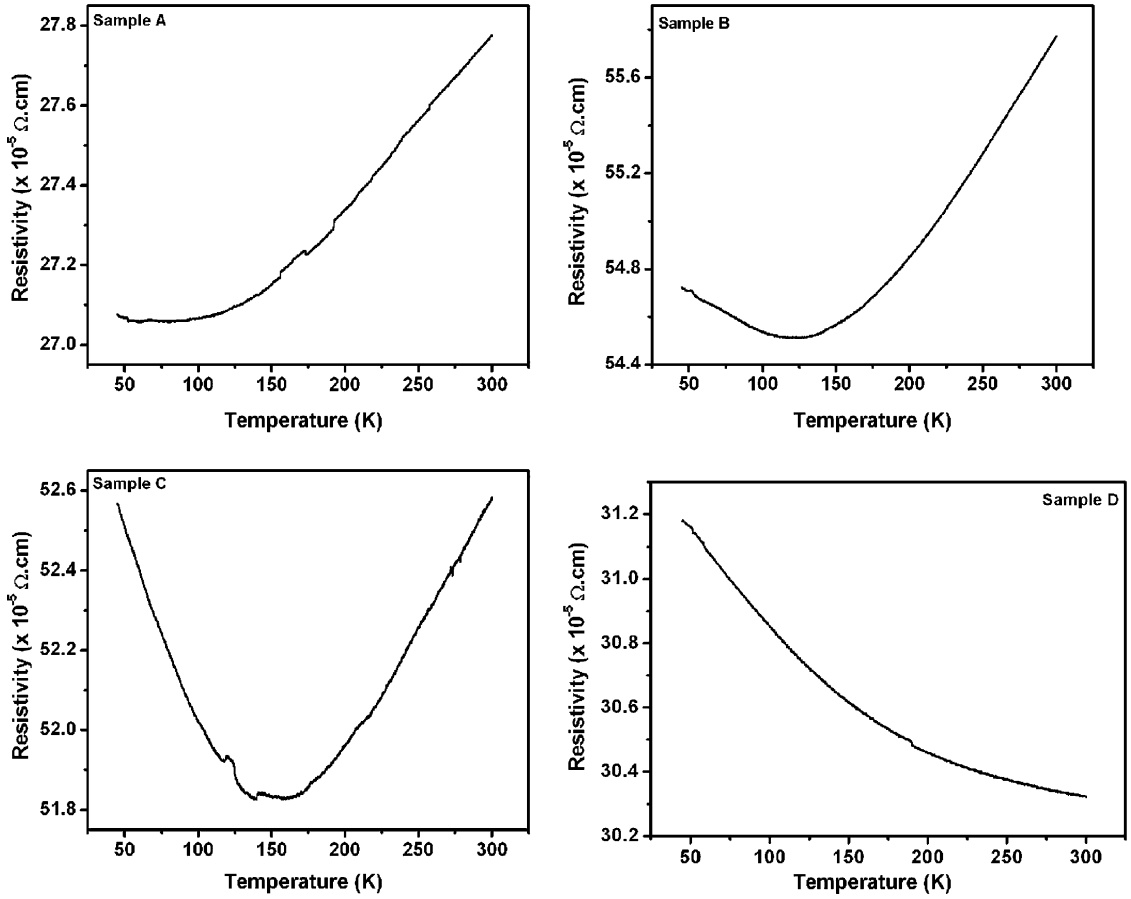

Fig. 7. Resistivity vs. temperature plots for film grown at (A) 7.5×10^{-6} Torr, (B) 7.5×10^{-5} Torr, (C) 7.5×10^{-4} Torr, and (D) 7.5×10^{-3} Torr of oxygen partial pressure.

tively. This suggests that two different mechanisms are responsible for electrical dc transport in the two temperature regions. The reason for this behavior is still unclear; however, it has been speculated that the positive TCR could be due to sintering of conducting clusters which form conducting paths through the sample [24]. The observed negative TCR at low temperatures is due to resistivity being dominated by ionized impurity scattering. The negative-to-positive TCR transition temperature in the films was observed to increase with partial oxygen pressure, which indicates that the films become more semiconducting and less metallic as corroborated by the decrease in carrier concentration in Fig. 6. Film grown at high partial oxygen pressure (Sample D) exhibits typical semiconducting behavior with negative TCR in the whole temperature region.

4. Conclusion

Structural, optical, and electrical transport properties of In_2O_3:Cr thin films have been investigated. Structural properties (lattice parameter and particle size) and transparency were found to be sensitive to oxygen growth pressure. Hall effect and temperature dependent resistivity measurements reveal that the electrical transport properties (carrier concentration, mobility, and resistivity) and mechanisms in these films can be effectively tuned by tuning the oxygen vacancies using oxygen pressure in the PLD chamber. Carrier mobility in the films was found out to increase with crystallinity while transparency decreased with increase in carrier concentration. Films deposited at low partial oxygen pressures – 7.5×10^{-6} Torr, 7.5×10^{-5} Torr, 7.5×10^{-4} Torr exhibited metallic behavior above approximately $T = 60$ K, $T = 120$ K, $T = 160$ K, respectively. The negative TCR to positive TCR transition temperature in these films was observed to increase with oxygen pressure. Film grown at high oxygen pressure displayed typical semiconducting behavior. Future magneto-transport studies of these films should reveal the exact nature of magnetic interactions especially for the films exhibiting metallic transitions.

Acknowledgement

Authors wish to acknowledge Prof. Ryan Giedd, Director of JVIC, Missouri State University for providing help to record AFM images and Raman Spectroscopy.

References

[1] D. Kumar, J. Antifakos, M.G. Blamire, Z.H. Barber, Appl. Phys. Lett. 84 (2004) 5004.
[2] J. Zhang, X.Z. Li, B. Xu, D.J. Sellmyer, Appl. Phys. Lett. 86 (2005) 212504.
[3] H. Ohno, H. Munekata, T. Penney, S. Molnar, L.L. Chang, Phys. Rev. Lett. 68 (1992) 2664.
[4] H. Munekata, H. Ohno, S. Molnar, A. Sergmuller, L.L. Chang, S. Esaki, Phys. Rev. Lett. 63 (1989) 1849.
[5] Y. Matsumoto, M. Murakami, T. Shono, T. Hasegawa, T. Fukumara, M. Kawasaki, P. Ahmet, T. Chikyow, S. Koshihara, H. Koinuma, Science 291 (2001) 854.
[6] K. Ueda, H. Tabata, T. Kawai, Appl. Phys. Lett. 79 (2001) 988.
[7] S.B. Ogale, R.J. Choudhury, J.P. Buban, S.E. Lofland, S.R. Shinde, S.N. Kale, V.N. Kulkarni, J. Higgins, C. Lanci, J.R. Simpson, N.D. Browning, S.D. Sarma, H.D. Drew, R.L. Greene, T. Venatesan, Phys. Rev. Lett. 91 (2003) 077205.
[8] J. He, S. Xu, Y.K. Yoo, Q. Xue, H.C. Lee, S. Cheng, X.D. Xiang, G. Dionne, I. Takeuchi, Appl. Phys. Lett. 89 (2004) 052503.
[9] J. Philip, A. Punnoose, B.I. Kim, K.M. Reddy, S. Layne, J.O. Holmes, B. Satpati, P.R. Leclair, T.S. Santos, J.S. Moodera, Nat. Mater. 5 (2006) 298.
[10] P. Kharel, C. Sudaker, M.B. Sahana, G. Lawes, R. Suryanarayanan, R. Naik, J. Appl. Phys. 101 (2007) 09H117.
[11] R.K. Gupta, K. Ghosh, S.R. Mishra, P.K. Kahol, Appl. Surf. Sci. 253 (2007) 9422.
[12] H.C. Pan, M.H. Shiao, C.Y. Su, C.N. Hsiao, J. Vac. Sci. Technol. A 23 (2005) 1187.
[13] Y. Abe, N. Ishiyama, Mater. Lett. 61 (2007) 566.
[14] A.A. Dakhel, Chem. Phys. Lett. 393 (2004) 528.
[15] H.K. Kim, C.C. Li, G. Nykolak, P.C. Becker, J. Appl. Phys. 76 (1994) 8209.
[16] A. Gupta, H. Cao, K. Parekh, K.V. Rao, A.R. Raju, U.V. Waghmare, J. Appl. Phys. 101 (2007) 09N513.
[17] R.K. Gupta, K. Ghosh, R. Patel, P.K. Kahol, J. Cryst. Growth 310 (2008) 4336.
[18] R.K. Gupta, K. Ghosh, S.R. Mishra, P.K. Kahol, Appl. Surf. Sci. 254 (2008) 4018.
[19] X.D. Zhou, W. Hueber, Appl. Phys. Lett. 79 (2001) 3512.
[20] R.K. Gupta, K. Ghosh, S.R. Mishra, P.K. Kahol, Appl. Surf. Sci. 254 (2008) 1661.
[21] S.T. Tan, B.J. Chen, X.W. Sun, W.J. Fan, H.S. Kwok, X.H. Zhang, S.J. Chua, J. Appl. Phys. 98 (2005) 013505.
[22] S. Tsunekawa, K. Ishikawa, Z.Q. Li, Y. Kawazoe, A. Kasuya, Phys. Rev. Lett. 85 (2000) 3440.
[23] J. Piour, S.D. Sarma, Phys. Rev. Lett. 97 (2006) 127201.
[24] J. Ederth, P. Johnsson, G.A. Niklasson, A. Hoel, A. Hultaker, P. Heszler, C.G. Granqvist, A.R. Doorn, M.J. Jongerius, Phys. Rev. B 68 (2003) 155410.